Spring 4-2-2018

Modeling and Simulation of Particle-Particle Interaction in a Magnetophoretic Bio-Separation Chip

Manjurul Alam

Matin Golozar

Jeff Darabi
jdarabi@siue.edu

Recommended Citation

Manjurul Alam, Matin Golozar, and Jeff Darabi, Modeling and simulation of particle-particle interaction in a Magnetophoretic bioseparation chip, Physics of Fluids 30, 042001 (2018); doi: 10.1063/1.5022582

Modelling and Simulation of Particle-Particle Interaction in a Magnetophoretic Bio-Separation Chip

Manjurul Alam, Matin Golozar, and Jeff Darabi
Department of Mechanical Engineering
Southern Illinois University Edwardsville
Edwardsville, Illinois 62026, USA

ABSTRACT

A Lagrangian particle trajectory model is developed to predict the interaction between cell-bead particle complexes and to track their trajectories in a magnetophoretic bio-separation chip. Magnetic flux gradients are simulated in OpenFOAM CFD software and imported into MATLAB to obtain the trapping lengths and trajectories of the particles. A connector vector is introduced to calculate the interaction force between cell-bead complexes as they flow through a microfluidic device. The interaction force calculations are performed for cases where the connector vector is parallel, perpendicular, and at an angle of 45 degrees with the applied magnetic field. The trajectories of the particles are simulated by solving a system of eight ordinary differential equations using a fourth order Runge-Kutta method. The model is then used to study the effects of geometric positions and angles of the connector vector between the particles as well as the cell size, number of beads per cell, and flow rate on the interaction force and trajectories of the particles. The results show that the interaction forces may be attractive or repulsive, depending on the orientation of the connector vector distance between the particle complexes and the applied magnetic field. When the interaction force is attractive, the particles are observed to merge and trap sooner than a single particle whereas a repulsive interaction force has little or no effect on the trapping length.

Keywords: Magnetic separation, particle-particle interaction, Lagrangian particle trajectory, Runge-Kutta method, cell-bead particle complexes, numerical simulation.

I. INTRODUCTION

Over the past two decades, microfluidic-based bioseparation devices have emerged as a viable technology to separate specific biological entities such as cells, bacteria, DNA/RNA, and proteins

This manuscript was accepted by Phys. Fluids. Click here to see the version of record.

from biological samples. These devices offer several advantages over conventional separation systems such as faster analysis, precise liquid handling, reduced amounts of reagents and samples, integration of multiple processes on a single chip, and portability. Among various microfluidic-based bioseparation techniques, magnetic-based systems are attractive due to their high selectivity, simplicity, and low cost. Magnetic bio-separation has been used in lab-on-a-chip devices, cell separators, micro-total analysis systems, and DNA/RNA isolators [1-11]. In this technique, the desired biological particles are labeled with specific magnetic beads, followed by isolating the marked entities by the use of a magnetic separation device.

Magnetic beads are comprised of iron oxide nanoparticles encapsulated in a polymer shell [12, 13]. The surface of the magnetic beads are coated with a specific ligand that has a strong affinity to the receptors on the surface of the bioparticles. The size of target bioparticles can range from ~5 μm - 50 μm for cells, 0.5 μm - 5 μm for bacteria, 20 nm - 450 nm for viruses, and 3 nm - 50 nm for proteins [14]. Due to a high degree of selectivity between magnetic particles and non-magnetic biomaterials, this separation method is more efficient than other bio-separation techniques. A significant number of analytical and experimental studies have been performed in the field of magnetophoretic bio-separation. A model has been developed by Nandy and Chaudhuri for the magnetophoretic capture of particles in a microfluidic device [15]. A magnetophoretic bio-separation chip has been designed, fabricated and modelled by Darabi and Guo [16]. This chip was developed to separate CD4+T cells from blood and was later used to separate DNA from blood [17]. Shevkoplyas et al. [18] performed a force analysis on a superparamagnetic bead in the presence of an applied magnetic field. Zhu et al. [19] fabricated a magnetic-based bio-separation chip using embedded permanent magnets. In a magnetic cell separation system, the cells and magnetic beads form cell-bead particle complexes. Since the cell size is usually larger than the magnetics beads, several micron-sized beads can bind to the surface of the cell to form a cell-bead complex. Depending on the number of beads attached to each cell, the effective mass, volume, density, and radius of the cell-bead complex can be estimated and used in force calculation analysis [20].

Particle-particle interaction force is an important phenomenon in a magnetophoretic bio-separation chip. This interaction can occur between particle complexes either through the magnetic

This manuscript was accepted by Phys. Fluids. Click here to see the version of record.

interaction force or the hydrodynamic interaction force [21-23]. In a magnetophoretic bio-separation technique, the interaction between particle complexes is mostly due to the magnetic moment produced by the individual particle complexes. Hence, hydrodynamic interaction force can be neglected. It has been reported that in a magnetophoretic bio-separation chip, magnetic particles tend to form chain-like structures [23], sheets [24], and membranes [25] due to the attractive magnetic force between the particles. Thus, particle-particle interaction must be considered because of its broad application in magnetic separation, magnetic drug targeting [26], and biomedical sensing [27]. Due to the interaction force between particles, the trapping length of a bonded particle complex is expected to be shorter than a single particle. In a microfluidic channel, the interaction force can be of a particular interest near the bottom of the channel where the induced magnetic dipole moment between the particles is larger. Some studies have been performed in the past to reduce the effect of particle-particle interaction at the bottom of the channel. Gao et al. [28] developed a model for disaggregation of superparamagnetic micro-particle complex clusters at the bottom of the channel with the help of induced magnetic dipole–dipole repulsion.

In this study, a dipole-based interaction force model was incorporated into the particle transport analysis in a magnetophoretic bio-separation chip and the effect of particle-particle interaction on particle trajectories was investigated. Magnetic flux gradients were simulated in OpenFOAM and particle transport modeling was performed in MATLAB by solving a system of eight coupled ordinary differential equations using a fourth order Runge-Kutta method.

II. THEORY

Two different approaches have been employed to obtain an analytical expression for the interaction force between magnetic dipoles [29]. These methods include a path integral approach and a vector differentiation approach. In both cases, the inter-particle distance vector is assumed to be large compared to the size of the dipoles. In classical electromagnetics, a magnetic field produced by a magnetic dipole is given by [30]

$$\vec{B}_{12} = -\frac{\mu_0}{4\pi}\left[\nabla\left(\frac{\vec{m}_1.\vec{r}}{r^3}\right)\right] \quad (1)$$

This manuscript was accepted by Phys. Fluids. Click here to see the version of record.

where m_1 is the magnetic dipole moment and r is the distance between the two dipoles, and μ_0 is the vacuum permeability. Using potential energy considerations, the force exerted by the dipole 1 on dipole 2 can be written as [31]

$$\vec{F}_{12} = \nabla\left(\vec{B}_{12}.\vec{m}_2\right) \tag{2}$$

By substituting the magnetic field equation into Eq. (2), the interaction force between the particles becomes [29]

$$\vec{F}_{12} = \frac{3\mu_0}{4\pi r^5}\left[(\vec{m}_1.\vec{r})\vec{m}_2 + (\vec{m}_2.\vec{r})\vec{m}_1 + (\vec{m}_1.\vec{m}_2)\vec{r} - \frac{5(\vec{m}_1.\vec{r})(\vec{m}_2.\vec{r})}{r^2}\vec{r}\right] \tag{3}$$

Where $\vec{F}_{12}$ is the interaction force, exerted on particle 1, $\vec{m}_1$ and $\vec{m}_2$ are the magnetic dipole moments of particles 1 and 2, and $\vec{r}$ is the connector vector between particles 1 and 2. Since the magnetic dipole moment is a function of the gradient of the magnetic field, it is difficult to have a good sense about the direction of the force. However, if the dipole moment is either parallel or perpendicular to the inter-particle distance vector, the force approximation will be simpler and an analytical expression can be obtained for the interaction force between two magnetic point dipoles [32-35]. A schematic illustration of magnetic dipole moments (m_1, m_2) of two cell-bead particle complexes under the influence of magnetic field is shown in Fig. 1. If the particles are assumed to be spherical point dipoles, the interaction force can be approximated by simplifying Eq. 1, depending on the direction of the magnetic moment. It is assumed that the particles do not rotate which is valid for cases where the magnetic dipole moment is either parallel or appendicular to the direction of the applied magnetic field. For a case where the magnetic moment is parallel to the inter-particle distance (Case I), Eq. 3 can be simplified as:

$$F_{12} = -\frac{3\mu_0}{2\pi r^4}(m_1.m_2) \tag{4}$$

The negative sign indicated that interaction force is attractive. If the particles are aligned parallel to the external applied field (i.e. $\theta = 0°$), they are attracted towards each other without any rotation because the magnetic interaction force and the external magnetic force are both parallel to the field direction. When the magnetic moment is perpendicular to the inter-particle distance (Case II), the interaction force is repulsive and is given by:

$$F_{12} = \frac{3\mu_0}{4\pi r^4}(m_1.m_2) \tag{5}$$

In this case, the particles are repelled from each other in the horizontal direction and descend in the vertical direction towards the bottom of the channel without any rotation because the magnetic

This manuscript was accepted by Phys. Fluids. Click here to see the version of record.

interaction force between the particles is only in the horizontal direction. For a case where the magnetic moment is at an angle of 45° with the inter-particle distance (Case III), Eq. 3 can be written as:

$$F_{12} = -\frac{3\mu_0}{4\pi r^4}(0.086 m_1 . m_2) \quad (6)$$

The interaction force is still attractive but it is significantly smaller than case I, where the magnetic moment is parallel to the inter-particle distance. In addition, for θ =45°, particles can rotate and change orientation inside the channel, but particle rotation is neglected in this work.

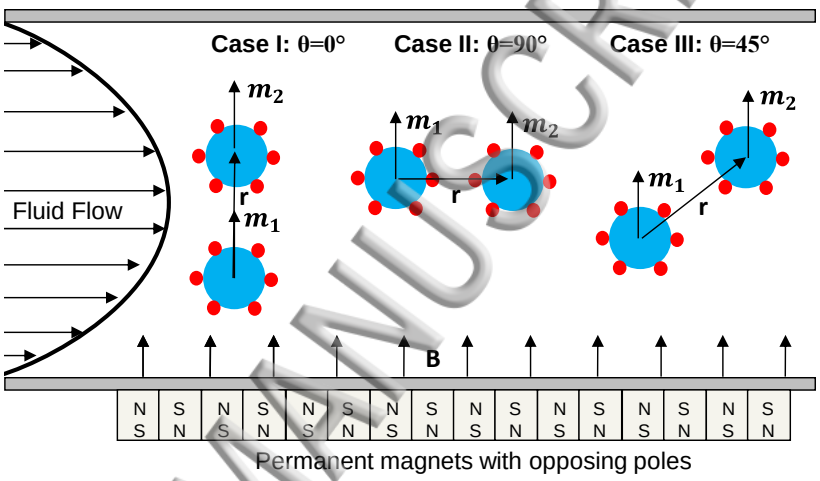

Figure 1 Schematic illustration of magnetic dipole moment (m_1, m_2) of two cell-bead particle complexes under the influence of the magnetic field in a magnetophoretic bio-separation chip. The schematic is not to scale.

Particle separation and transport is an important phenomenon in many microfluidic devices. Figure 2 shows a schematic illustration of different forces acting on two cell-bead particle complexes in the presence of an applied magnetic field as they move along the channel. Among the various forces acting on the particles, the magnetic force, gravitational force, hydrodynamic drag force, and inter-particle interaction force are the dominant forces. The effects of Brownian motion can be ignored since the size of the particles in this study is in the 10-30 micron range. Van der Waals force was also neglected due to the size and concentration of the particles used in this analysis [36].

This manuscript was accepted by Phys. Fluids. Click here to see the version of record.

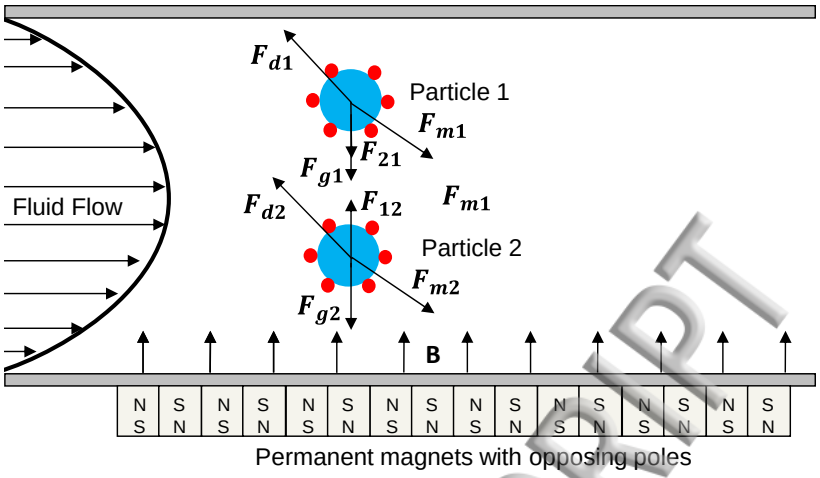

Figure 2 Schematic illustration of different forces acting on two cell-bead particle complexes subjected to an applied magnetic field. Hydrodynamic drag force, gravitational force, magnetic force, and inter-particle interaction force are considered in the computational analysis. The schematic is not to scale.

A solid particle suspended in a fluid experiences a hydrodynamic drag force opposite to its direction of motion. If the Reynolds' number is low, which is the case with most microfluidic devices, the hydrodynamic drag force on a spherical particle can be approximated by Stokes' law:

$$\vec{F}_d = 6\pi R_p \eta (\vec{V}_f - \vec{V}_p) \tag{7}$$

Where R_p is the particle radius, η is the dynamic viscosity of the medium, and $\vec{V}_f$ and $\vec{V}_p$ are the fluid and particle velocities, respectively. If the flow is laminar, the velocity distribution across the channel can be determined by solving a steady flow between two parallel plates as follows:

$$\vec{V}_f = 6\frac{\mathrm{Q}}{\mathrm{hw}}\left(\frac{\mathrm{y}}{\mathrm{h}} - \left(\frac{\mathrm{y}}{\mathrm{h}}\right)^2\right)\vec{\imath} \tag{8}$$

Where Q is the volumetric flow rate, h is the channel height, and w is the channel width. Stokes drag force can be modified for non-spherical particles such as a chain of small spheres [37]. In such case, the drag force equation can be written as:

$$\vec{F}_d = 6\pi R_{pe} \eta k (\vec{V}_f - \vec{V}_p) \tag{9}$$

where k is a shape factor and R_{pe} is the equivalent radius of a sphere having the same volume as the chain of small spheres,

This manuscript was accepted by Phys. Fluids. Click here to see the version of record.

$$R_{pe} = \sqrt[3]{\frac{3v_{pe}}{4\pi}} \tag{10}$$

For a cluster of n spheres,

$$R_{pe} = n^{\frac{1}{3}} R_p \tag{11}$$

The magnetic force acting on a particle complex is a function of the magnetic moment of each magnetic particle, number of beads attached to the cell, and magnetic field gradients:

$$\vec{F}_m = N(\vec{m}_b.\nabla)\vec{B} \tag{12}$$

where $\vec{m}_b$ is the magnetic dipole moment of the bead, N is the number of beads, $\vec{B}$ is the magnetic field. Magnetic moment of the beads can be written as:

$$\vec{m}_b = \rho_b V_b \vec{M}_b \tag{13}$$

where ρ_b, V_b and $\vec{M}_b$ are the density, volume, and magnetization of the bead, respectively. At very low flow rates, the gravitational force can have an effect on trapping efficiency of a particle in a magnetic bio-separation chip. Thus, the gravitational force should be taken into account in the analysis of particle transport. The net gravitational force is due to the density difference between the particle and fluid. Thus, the net gravitational force can be written as:

$$\vec{F}_g = (\rho_p - \rho_f) v_p \vec{g} \tag{14}$$

where ρ_p and ρ_f are the densities of the particle and fluid, respectively, v_p is the volume of the particle, $\vec{g}$ is the gravitational acceleration.

III. MATERIALS AND METHODS

A. Modelling and Simulation

OpenFOAM CFD software was used to simulate magnetic flux gradients above an array of external magnets with opposing poles. A detailed description of the magnetic field simulations has been previously reported and it is not repeated here for brevity [38]. The magnetic flux gradients were then imported into MATLAB to calculate the magnetic force at various nodes inside the microfluidic channel. Figures 3-5 show representative magnetic force distributions at various distances from the surface of the magnets for an array of eight permanent magnets configured in an alternating polarity along the channel. Figure 3 shows the variation of the x-component of the magnetic force, $F_{m,x}$, along the channel at various distances from the surface of the magnets. Due to the alternating polarity arrangement of the magnets, $F_{m,x}$ changes direction from one magnet to

This manuscript was accepted by Phys. Fluids. Click here to see the version of record.

another. This oscillatory feature of the magnetic force in x-direction is more visible near the surface of the magnets and as the distance from the magnets increases to 800 µm away from the surface, the magnetic force becomes relatively negligible.

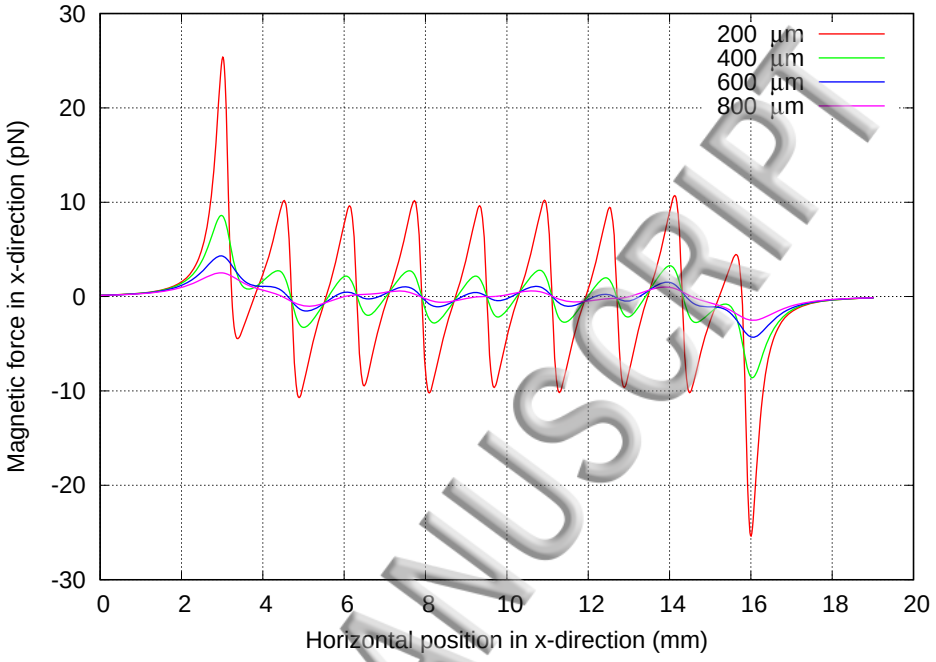

Figure 3 Variation of the x-component of the magnetic force along the channel at various distances from the surface of the magnets.

Figure 4 depicts the variation of the y-component of the magnetic force, $F_{m,y}$, along the channel at various distances from the surface of the magnets. The negative sign indicates that the direction of $F_{m,y}$ is towards the surface of the magnets. Furthermore, by comparing $F_{m,x}$ and $F_{m,y}$ values, it can be concluded that the dominant component of the magnetic force inside the channel is the y component of the force, which is approximately 5 times larger than $F_{m,x}$. The norm of the magnetic force along the channel at different distances from the surface of the magnets is shown in Figure 5. It can be seen from this figure that the magnetic force is substantially higher at the interface of the magnets. Due to polarity arrangement of the magnets, the force produced inside the channel is

ager than a single magnet and it provides net magnetic force on the particle at a distance of 600 μm from the surface of the magnets is approximately 10-15 pN.

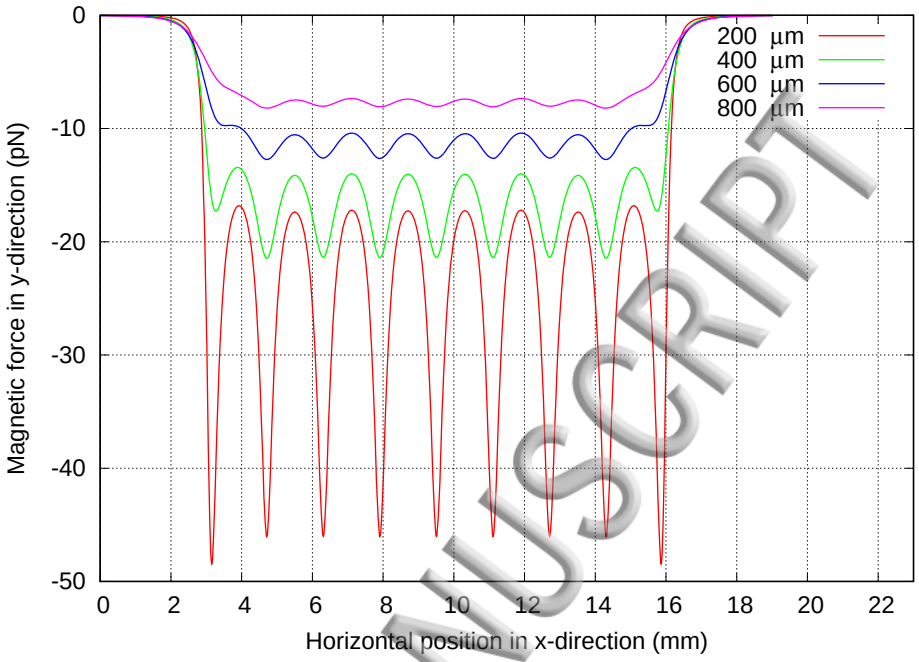

Figure 4 Variation of the y-component of the magnetic force along the channel at various distances from the surface of the magnets.

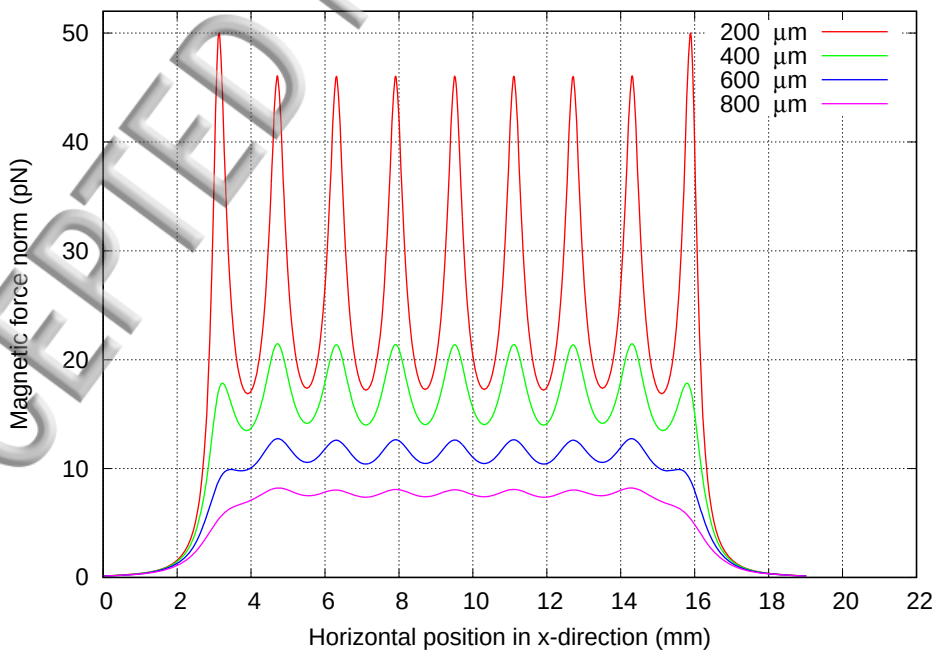

This manuscript was accepted by Phys. Fluids. Click here to see the version of record.

Figure 5 Variation of magnetic force norm along the channel at various distances from the surface of the magnets.

In this work, horizontal and vertical components of the magnetic force along with the drag force, gravitational force, and particle-particle interaction force were used to predict particle trajectories inside the fluidic channel. When the magnetic moment is parallel to the connector vector, the motion of the particles in the channel can be predicted by applying Newton's second law in the x and y directions as follows:

Force balance for particle 1 in the x-direction:

$$m_{p1}\frac{dv_{p1,x}}{dt} = F_{d1,x} + F_{m1,x} \tag{15}$$

Force balance for particle 1 in the y-direction:

$$m_{p1}\frac{dv_{p1,y}}{dt} = F_{d1,y} + F_{m1,y} + F_{g1} + F_{21} \tag{16}$$

Force balance for particle 2 in the x-direction:

$$m_{p2}\frac{dv_{p2,x}}{dt} = F_{d2,x} + F_{m2,x} \tag{17}$$

Force balance for particle 2 in the y-direction:

$$m_{p2}\frac{dv_{p2,y}}{dt} = F_{d2,y} + F_{m2,y} + F_{g2} + F_{12} \tag{18}$$

Substituting equations 4-9 and 11 in equations 15-18, and simplifying, we can write:

$$\frac{dv_{p1,x}}{dt} + kv_{p1,x} = n_{1x} \tag{19}$$

$$\frac{dv_{p1,y}}{dt} + kv_{p1,y} = n_{1y} \tag{20}$$

$$\frac{dv_{p2,x}}{dt} + kv_{p2,x} = n_{2x} \tag{21}$$

This manuscript was accepted by Phys. Fluids. Click here to see the version of record.

$$\frac{dv_{p2,y}}{dt} + kv_{p2,y} = n_{2y} \tag{22}$$

Where

$$k = \frac{6\pi R_{p1}\boldsymbol{\eta}}{m_{p1}} = \frac{6\pi R_{p2}\boldsymbol{\eta}}{m_{p2}} \tag{23}$$

$$n_{1x} = \frac{36\pi R_{p1}\eta Q}{m_{p1}hw}\frac{y}{h}\left(1-\frac{y}{h}\right) + \frac{N\rho_b V_b m_{sat}\left(\frac{\partial B_x}{\partial x}+\frac{\partial B_x}{\partial y}\right)}{m_{p1}} \tag{24}$$

$$n_{1y} = \frac{N\rho_b V_b m_{sat}\left(\frac{\partial B_y}{\partial x}+\frac{\partial B_y}{\partial y}\right)+(\rho_p-\rho_f)v_{p1}g+\frac{3\mu_0}{2m_{p1}\pi D^4|r/D|^4}(-m_1m_2)}{m_{p1}} \tag{25}$$

$$n_{2x} = \frac{36\pi R_{p2}\eta Q}{m_{p2}hw}\frac{y}{h}\left(1-\frac{y}{h}\right) + \frac{N\rho_b V_b m_{sat}\left(\frac{\partial B_x}{\partial x}+\frac{\partial B_x}{\partial y}\right)}{m_{p2}} \tag{26}$$

$$n_{2y} = \frac{N\rho_b V_b m_{sat}\left(\frac{\partial B_y}{\partial x}+\frac{\partial B_y}{\partial y}\right)+(\rho_p-\rho_f)v_{p2}g+\frac{3\mu_0}{2\pi D^4|r/D|^4}(-m_1m_2)}{m_{p2}} \tag{27}$$

Equations 19-22 constitute a system of coupled ordinary differential equations (ODEs). When the applied magnetic field is parallel to the connector vector, the coupled system of equations can be written as:

$$\frac{dv_{p1,x}}{dt} = n_{1x} - kv_{p1,x} \tag{28}$$

$$v_{p1,x} = \frac{dx_1}{dt} \tag{29}$$

$$\frac{dv_{p1,y}}{dt} = n_{1y} - kv_{p1,y} \tag{30}$$

This manuscript was accepted by Phys. Fluids. Click here to see the version of record.

$$v_{p1,y} = \frac{dy_1}{dt} \tag{31}$$

$$\frac{dv_{p2,x}}{dt} = \mathrm{n_{2x}} - \mathrm{kv_{p2,x}} \tag{32}$$

$$v_{p2,x} = \frac{dx_2}{dt} \tag{33}$$

$$\frac{dv_{p2,y}}{dt} = \mathrm{n_{2y}} - \mathrm{kv_{p2,y}} \tag{34}$$

$$v_{p2,y} = \frac{dy_2}{dt} \tag{35}$$

The simulations were performed using a 4th order Runge-Kutta method. Equations 28-35 were solved subject to initial conditions for position of $x_1(0)$, $y_1(0), x_2(0), y_2(0)$ and velocity of $v_{p1,x}(0)$, $v_{p1,y}(0)$, $v_{p2,x}(0)$, $v_{p2,y}(0)$ of the particles. Then, the change in the vertical and horizontal positions of the particles were calculated from the initial position where the particles started their transports in the channel to determine the particle trajectories within the microfluidic channel. Similar analyses were performed for cases where the applied magnetic field was perpendicular or at an angle of 45° to the connector vector. The flowchart of the solution algorithm is shown in Fig. 6.

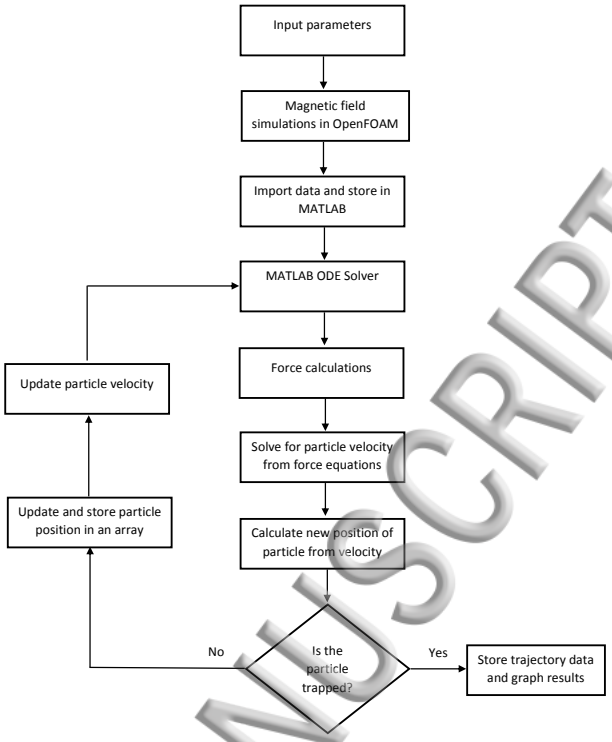

Figure 6 A flowchart of numerical simulation

B. Experimental Method

Since the resolution of optical microscopy is not suitable for tracking of small and fast-moving particles inside a microfluidic channel, it is not possible to experimentally control and measure the trajectories of cell-bead complexes. Thus, to verify the computational model, a series of experiments were carried out using 1-µm superparamagnetic beads at various flow rates and their trapping lengths were experimentally measured. The trapping length refers to the farthest distance a particle can travel before it is captured on the bottom of the channel. For example, if the channel height is 200 µm and the particle starts its journey from the top of the channel, it slowly descends towards the bottom of the channel due to the magnetic force as it travels through the channel. Once the particle reaches the bottom of the channel, the particle is considered as being trapped. The horizontal distance that the particle travels from its starting position until it is trapped on the bottom of the channel is referred to as the trapping length of the particle.

Figure 7 shows a photograph of the experimental setup which consists of a bidirectional MilliGat pump with a MicroLynx controller for the sample, a syringe pump for the buffer, an optical microscope to monitor the particle motion within the channel, and plastic tubing for the connections between the pumps and the chip. Magnetic bead samples were prepared by washing and diluting a 10 µL concentrated magnetic beads in 990 µL deionized water (a 1:100 dilution). Before introducing the sample into the channel, the chip and tubing were washed with deionized water and soaked with 20 % bovine serum albumin (BSA) for 30 minutes and rinsed with the isolation buffer. Next, the diluted bead sample was injected into the separation channel using a bidirectional milliGAT pump. The flow rate was varied from 10 mL/h to 80 mL/h in 10 mL/h increments. Each test was repeated three times and the average values of the trapping length of superparamagnetic beads were measured.

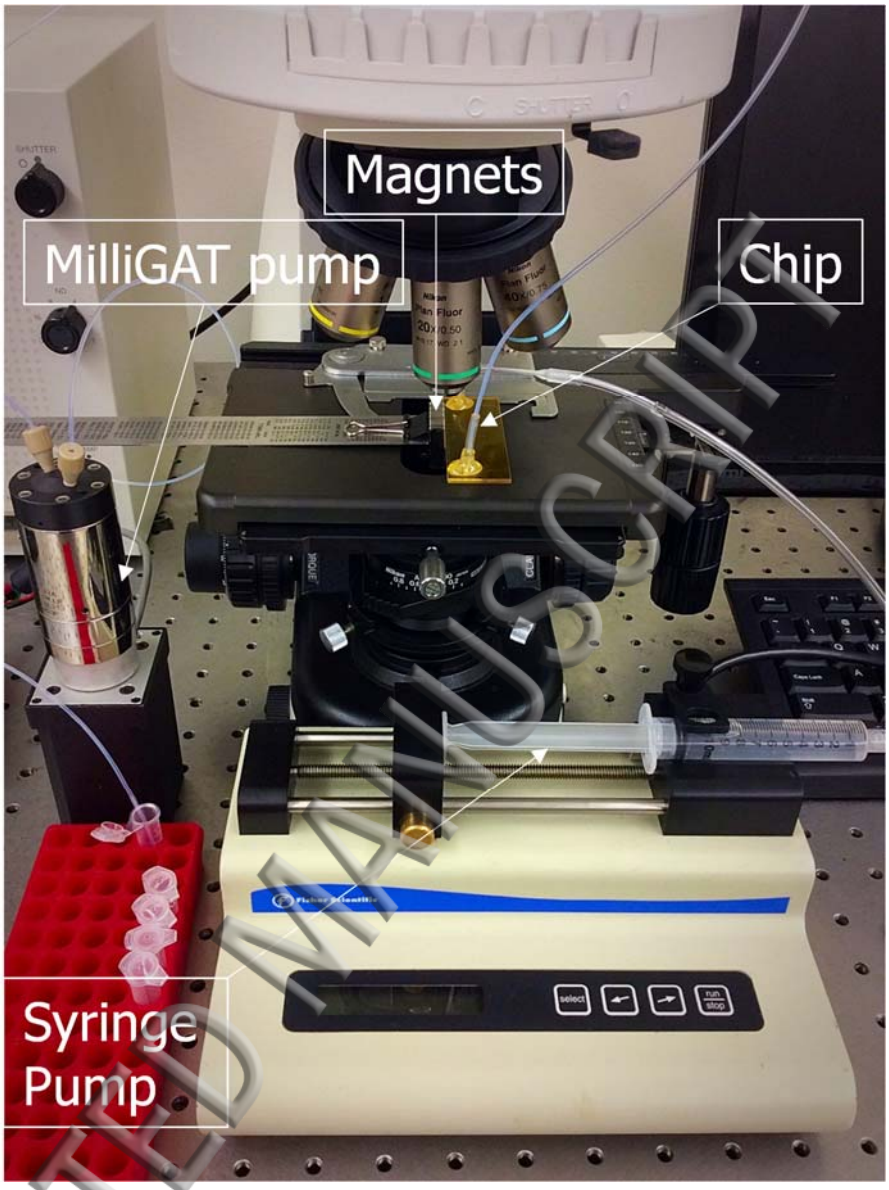

Figure 7 A photograph of the experimental setup

IV. RESULTS AND DISCUSSION

Figure 8 shows a comparison between the experimentally measured and simulated trapping lengths at various flow rates. The simulated trapping lengths were found to be in good agreement with the experimental results confirming our modeling approach and methodology. Once the model was validated for superparamagnetic beads, simulations were performed to determine the trajectories of two cell-bead particle complexes for the following three cases:

1) Case I: The applied magnetic field is parallel (0°) to the connector vector.

2) Case II: The angle between the applied magnetic field and the connector vector is 45°.

3) Case III: The applied magnetic field is perpendicular (90°) to the connector vector.

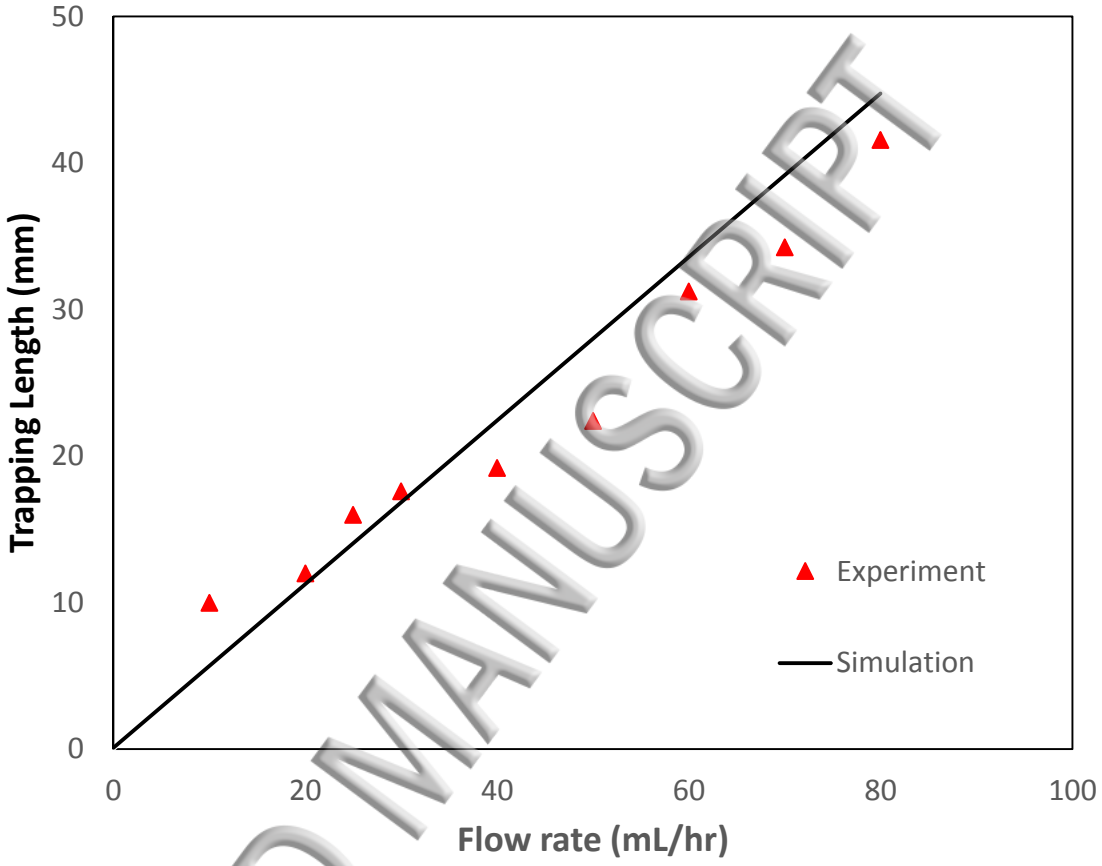

Figure 8 A comparison between the simulated and experimentally measured trapping length of 1-μm superparamagnetic beads at various flow rates

The 0° (parallel) and 90° (perpendicular) cases were selected because they represent extreme situations where particles either fully attract or fully repel one another. If the cell-bead complexes are aligned parallel to the external applied field, the magnetic interaction force between the particles is attractive, causing the cell-bead complexes to merge together and eventually trap earlier at the bottom of the channel. On the other hand, if the connector vector between complexes is perpendicular to the direction of magnetic field, the magnetic interaction force is repulsive, forcing the particles to move away from one another. In this case, the particles do not merge and follow their own trajectories inside the channel until they are trapped or flow out of the channel. While one could model any angles between 0 and 90 degree, we selected for a 45 degrees angle because

This manuscript was accepted by Phys. Fluids. Click here to see the version of record.

the interaction force is still attractive albeit much weaker than the zero degrees case but it results in a shorter trapping length. The angles that results in a repulsive force do not lead to interesting results because it has very little or no effect on particle trajectory and each particle follows its own trajectory.

Simulations were performed to study the effects of sample flow rate, number of beads per cell, and cell size on the trajectory of the cell-bead complexes by taking into account the particle-particle interaction. The inter-particle distance (center to center distance between the particles) was also varied to investigate its effect on the interaction force and particle trajectories. Figure 9 depicts the effect of flow rate on trajectories of two cell-bead particle complexes as they travel along the channel. The number of beads per cell, cell size, and bead size are 10, 10 μm, and 1 μm, respectively. The inter-particle distance was assumed to be twice the particle diameter. Each set of two lines with the same color represent the trajectories of two identical particles that start their journeys from two different initial positions while they are slowly attracted and eventually merged together due to the particle-particle interaction force. The point where the two lines with the same color merge represents the position where the particles join together. From that point on, the merged particles are considered as a single particle and follows its own trajectory inside the channel. The bonded particle is observed to descend at a much steeper slope within the microfluidic channel until it is finally trapped on the bottom of the channel. This is because when the particles are joined together, their magnetic moments increase by a factor of two since the magnetic moment is linearly proportional to the number of beads, but the drag force does not increase linearly. Since the bonded particle is not spherical, a shape factor was introduced to calculate the drag force by assuming that the bonded particles form a chain-like cluster of spheres. A shape factor value of k=1.12 was used in the simulation because the chain is aggregate of two spherical particles [37]. Other parameters of particle modelling remains the same but the effective mass and volume are twice that of a single particle.

The results also show that the external magnetic force is stronger than the interaction force between the particles. For example, by the time that the particles with an initial distance of 20 μm are attracted and merged together due to the interaction force, they descend by more than 50 μm due to the external magnetic field. The results also indicate that the particle trapping length increases

This manuscript was accepted by Phys. Fluids. Click here to see the version of record.

with increasing the flow rate. This is because as the flow rate increases, the particle velocity along the channel increases as well, but the external magnetic force remains constant. As a result, the particle travels a longer distance before it is trapped on the bottom of the channel.

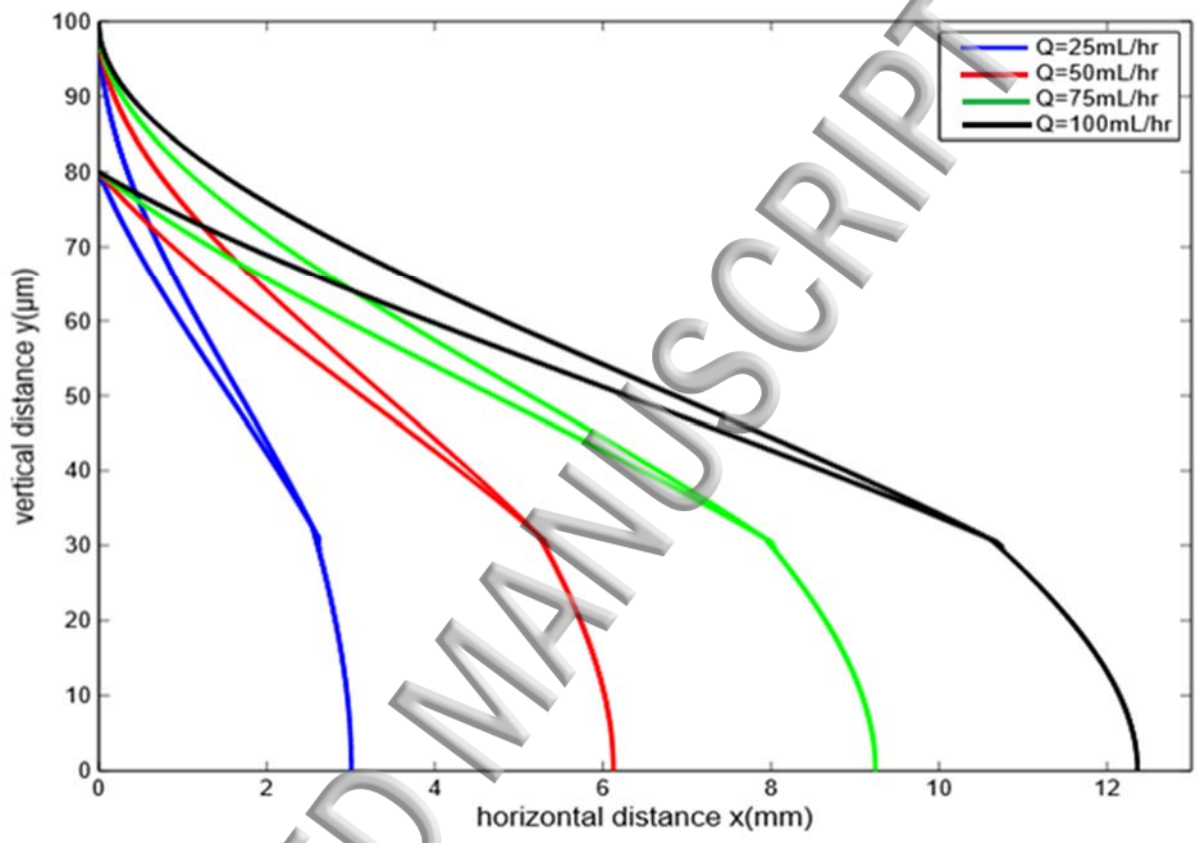

Figure 9 Trajectories of two cell-bead particle complexes at various flow rates for a case where the applied magnetic field is parallel to the connector vector. The distance between particle complexes is twice the particle diameter (r=2D).

In a magnetophoretic bio-separation chip, the number of beads that are attached to each cell can have a significant effect on particle-particle interaction. Figure 10 shows the simulation results for an inter-particle spacing of r=2D at various number of beads per cell. The cell size, bead size, and flow rate are 10 μm, 1 μm, and 50 mL/hr, respectively. The particles are assumed to start from the same horizontal position at the same time, but the first particle starts its journey from a vertical position of 100 μm while the second particle starts from a vertical position of 80 μm. The results indicate that the trapping length decreases with increasing the number of beads per cell. This is due to the fact that as the number of beads per cell increases, the magnetic moment of the particle

This manuscript was accepted by Phys. Fluids. Click here to see the version of record.

complexes increase as well. As a result, the particle complexes with more number of beads are attracted to each other at a much faster rate and bonded together sooner. Additionally, particles with more number of beads descend at a faster rate because as shown in Eq. (12), the external magnetic force is proportional to the number of beads.

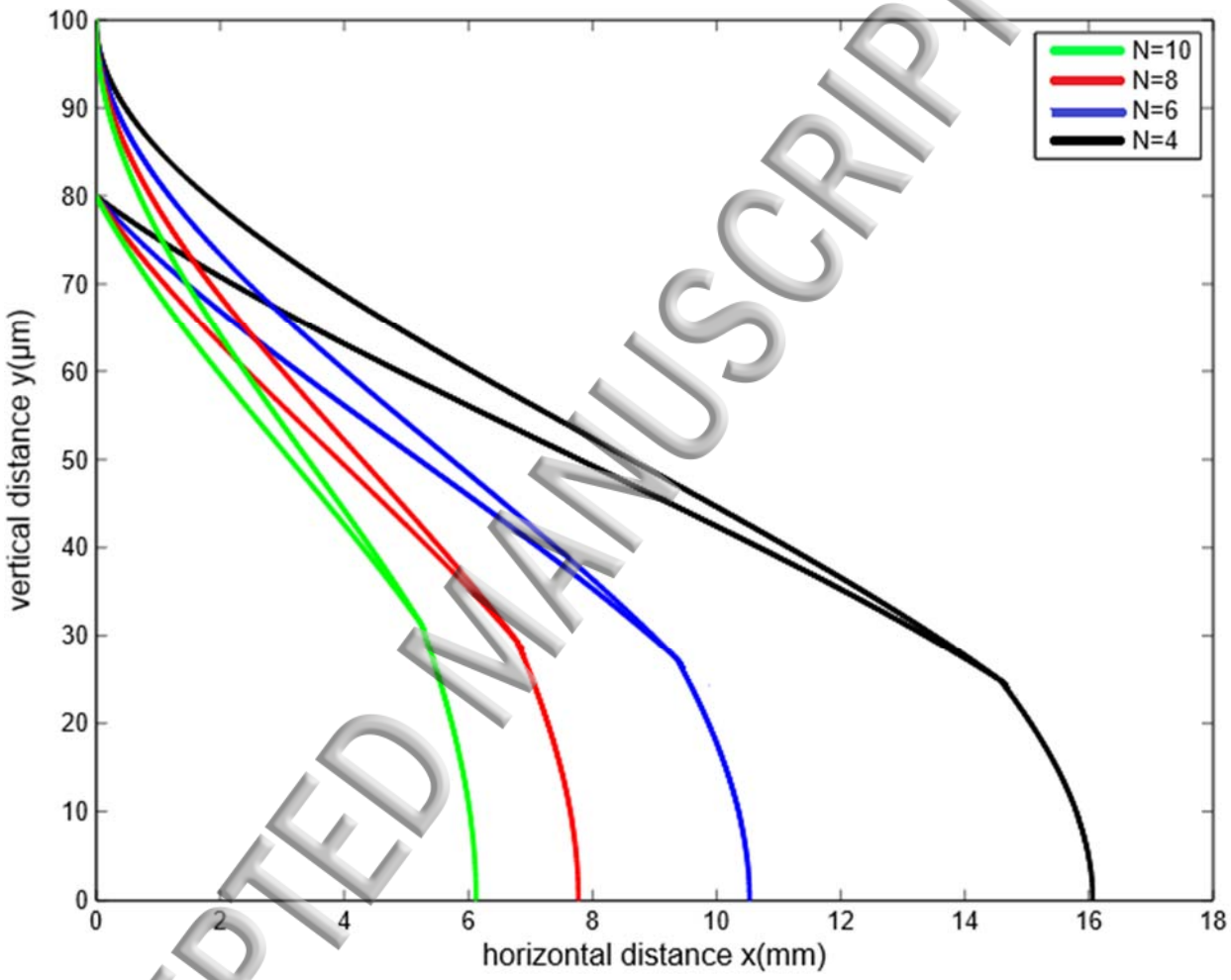

Figure 10 Trajectories of two cell-bead particle complexes at various number of beads per cell for a case where the applied magnetic field is parallel to the connector vector. The distance between particle complexes is twice the particle diameter (r=2D).

For a given number of beads per cell, the interaction force between particle complexes is different depending on the cell size. Figure 11 shows the particle trajectories for three different cell sizes at an inter-particle distance of r=2D. The flow rate, number of beads, and bead size are 50 mL/hr, 10, and 1 μm, respectively. In all cases, as the particles travel along the channel, they are attracted

towards each other due to an attractive interaction force and eventually form a single bonded particle. It is observed that as the cell size increases, it takes more time for the particles to be trapped on the bottom of the channel. This is because the drag force is greater on a larger particle, causing the particle to move at a slower velocity. Thus, if the number of beads per cell is kept the same, it can be said that the particle interaction is less dominant for larger cell sizes.

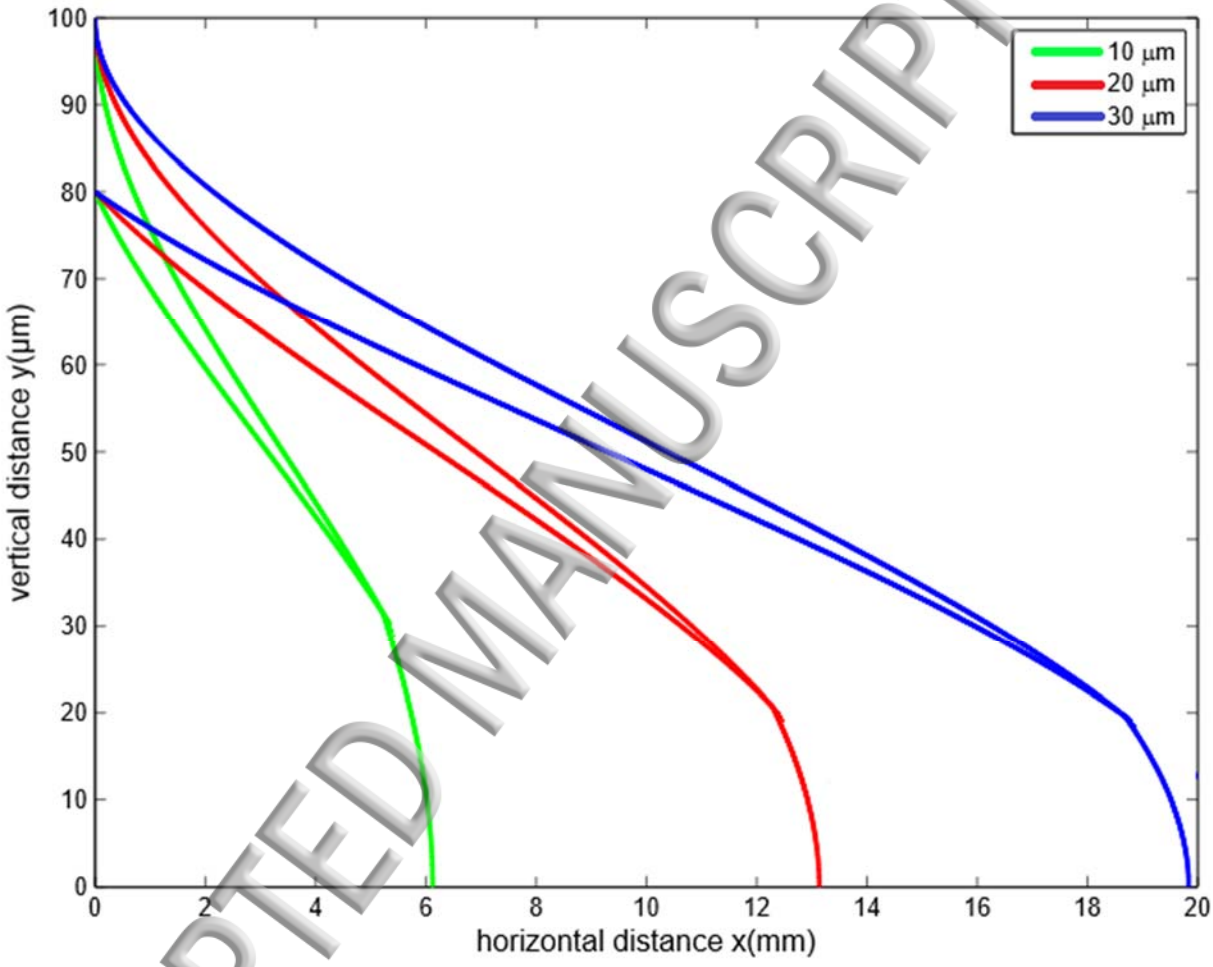

Figure 11 Trajectories of two cell-bead particle complexes at various cell sizes for a case where the applied magnetic field is parallel to the connector vector. The distance between particle complexes is twice the particle diameter (r=2D).

Figure 12 depicts the trajectories of two cell-bead particle complexes for a case where the applied magnetic field is parallel to the connector vector at two different inter-particle distances of r=D and r=2D. The number of beads per cell, cell size, bead size, and flow rate are 10, 10 µm, 1 µm, 50 mL/hr, respectively. The trajectory of a single particle is also plotted for comparison. Note that for the r=D case, one particle starts its journey from a vertical position of 100 µm while the other

particle starts from a vertical position of 90 µm. For the r=2D case, one particle starts from a vertical position of 100 µm while the other particle starts from a vertical position of 80 µm. It is observed that for the r=D case, the bonded particle is trapped sooner on the bottom of the channel compared to the r=2D and single particle cases. The results also indicate that as the inter-particle distance increases, it will take a longer time for the particle complexes to get closer and bond together. This is because the interaction force decreases as the distance between the particle complexes increases. Once the particles are pulled together and bonded, the magnetic force will be higher than the hydrodynamic drag force. Thus, the trapping of the bonded particle accelerate for the r=D case. Simulations were also performed for a case where the distance between particle complexes was three times the particle diameter (i.e. r=3D). At this particular inter-particle distance, the interaction force was not sufficient to pull the particles together and each particle followed its own trajectory. As the particles moved along the channel, the inter-particle distance was observed to decrease but the interaction force was not sufficient to change the trajectories of individual particles significantly. These results are not shown because the trajectories were similar to a single particle trajectory.

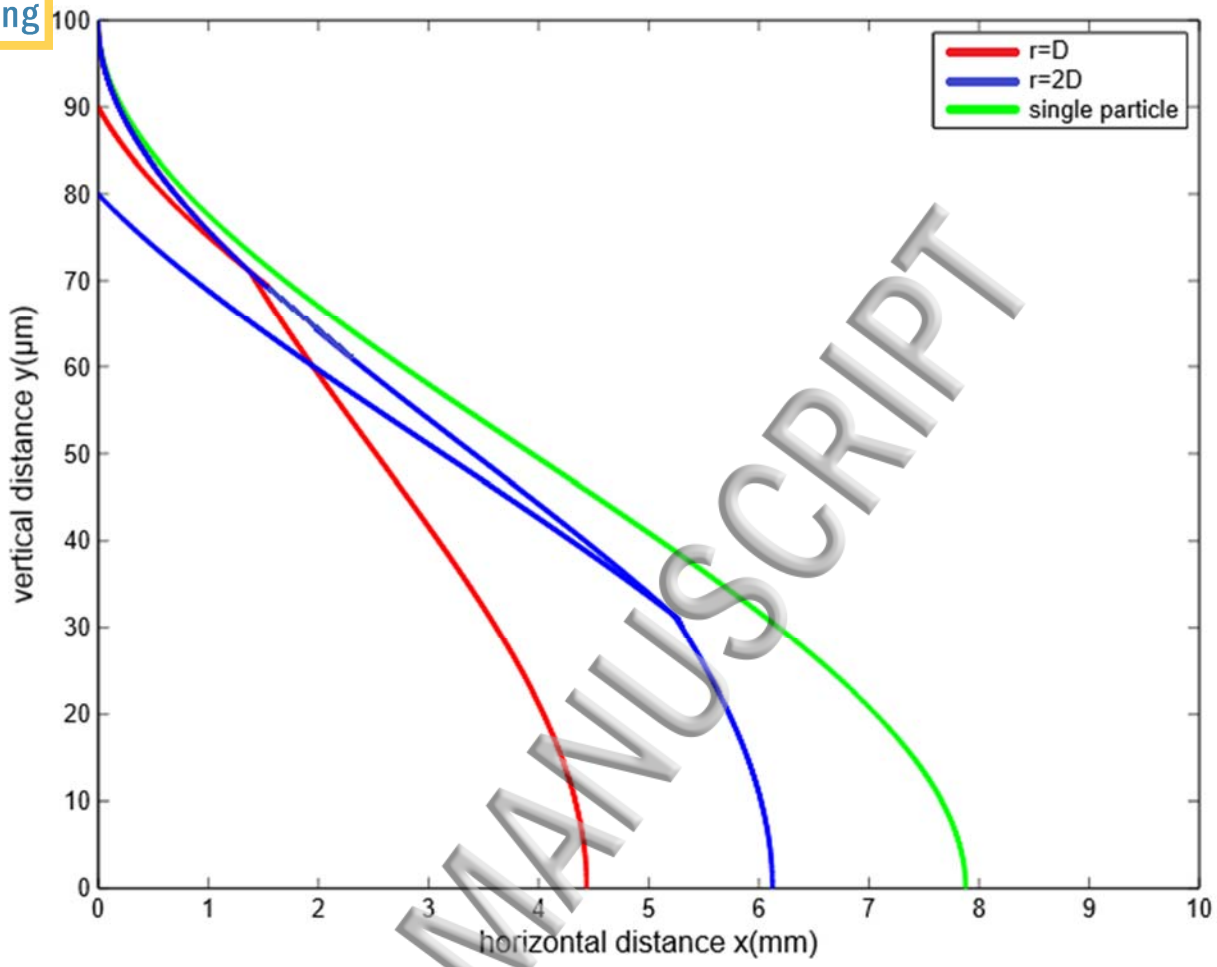

Figure 12 Trajectories of two cell-bead particle complexes at various inter-particle distances for a case where the applied magnetic field is parallel to the connector vector. The trajectory of a single particle is shown for comparison.

Simulations were also performed for case II, where the magnetic field is perpendicular to the connector vector distance. Figure 13 shows the trajectories of two cell-bead particle complexes for an inter-particle distance of r=2D. The number of beads per cell, cell size, bead size, flow rate are 10, 10 μm, 1 μm, and 50 mL/hr, respectively. It is observed that the particles are not attracted to each other in this case and each particle follows its own trajectory. This is because as shown in Equation 5, when the connector vector is perpendicular to the magnetic moment, the interaction force between the particles is repulsive, causing particles to move away from each other. In this case, the particle-particle interaction force has a very little or no effect on the trapping length.

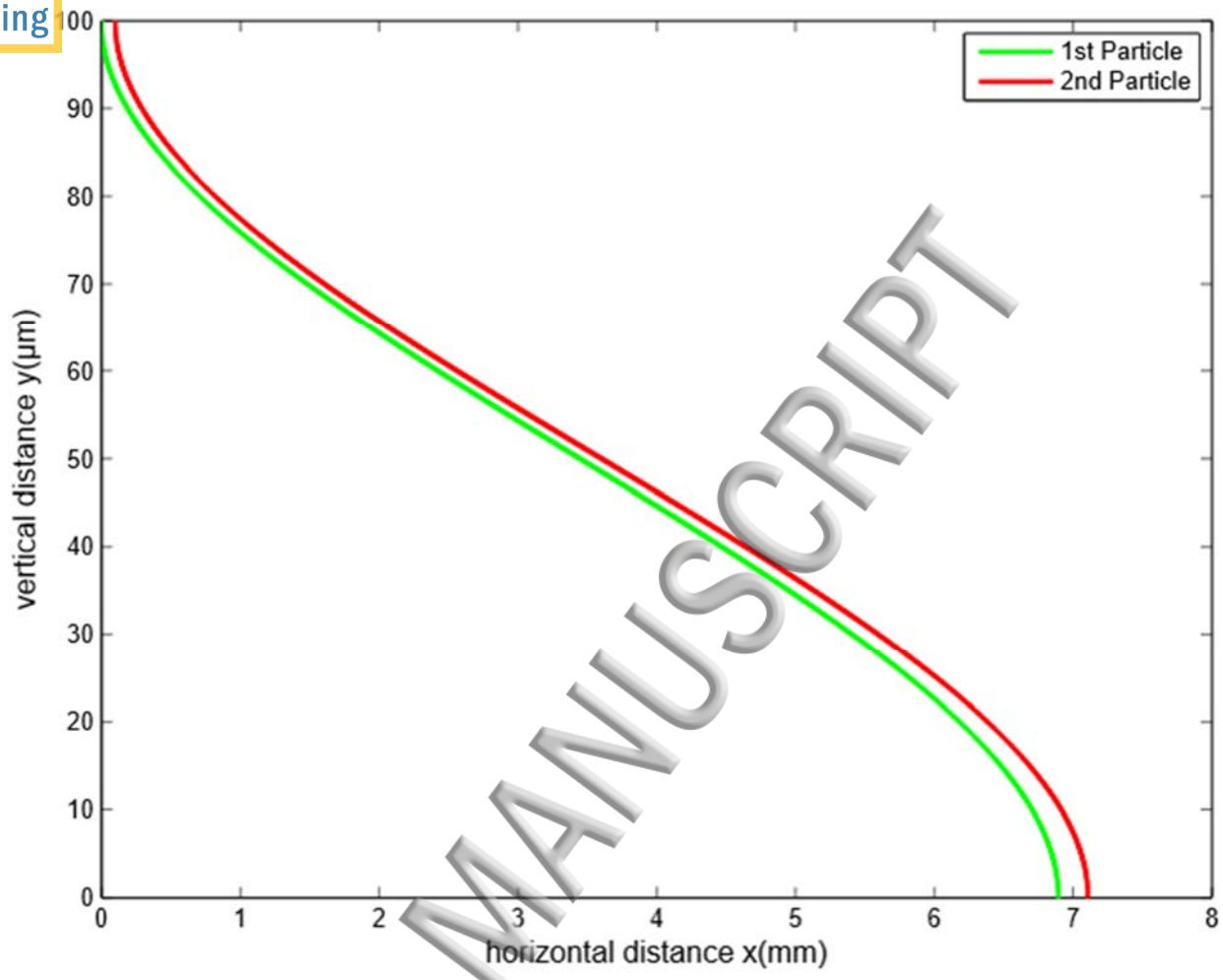

Figure 13 Trajectories of two cell-bead particle complexes for a case where the applied magnetic field is perpendicular to the connector vector.

Figure 14 depicts a comparison between the trajectories of particle complexes for cases where the applied magnetic field is parallel (0°) or forms a 45° angle with the connector vector. A single particle trajectory, which is similar to the case where the magnetic field is perpendicular to the connector vector (i.e. 90°) is also plotted for comparison. In all cases, the cell size, bead size, number of beads, and flow rate are 10 μm, 1 μm, 10, and 50 mL/hr, respectively. The results show that the trapping length for the 0° case is shorter than the 45° case and the 45° case is shorter than the single particle trapping length. This is because the particle-particle interaction force for the 0° case is much stronger than the 45° case as shown in Eqs. 4 and 6. In addition, as the particle complexes move along the channel, they are attracted towards each other and eventually stick together. Since the manganic moment of the merged particle is larger than each individual particle,

This manuscript was accepted by Phys. Fluids. Click here to see the version of record.

the descending velocity of the bonded particle increases, resulting in a shorter trapping length for the merged particles compared to a single particle.

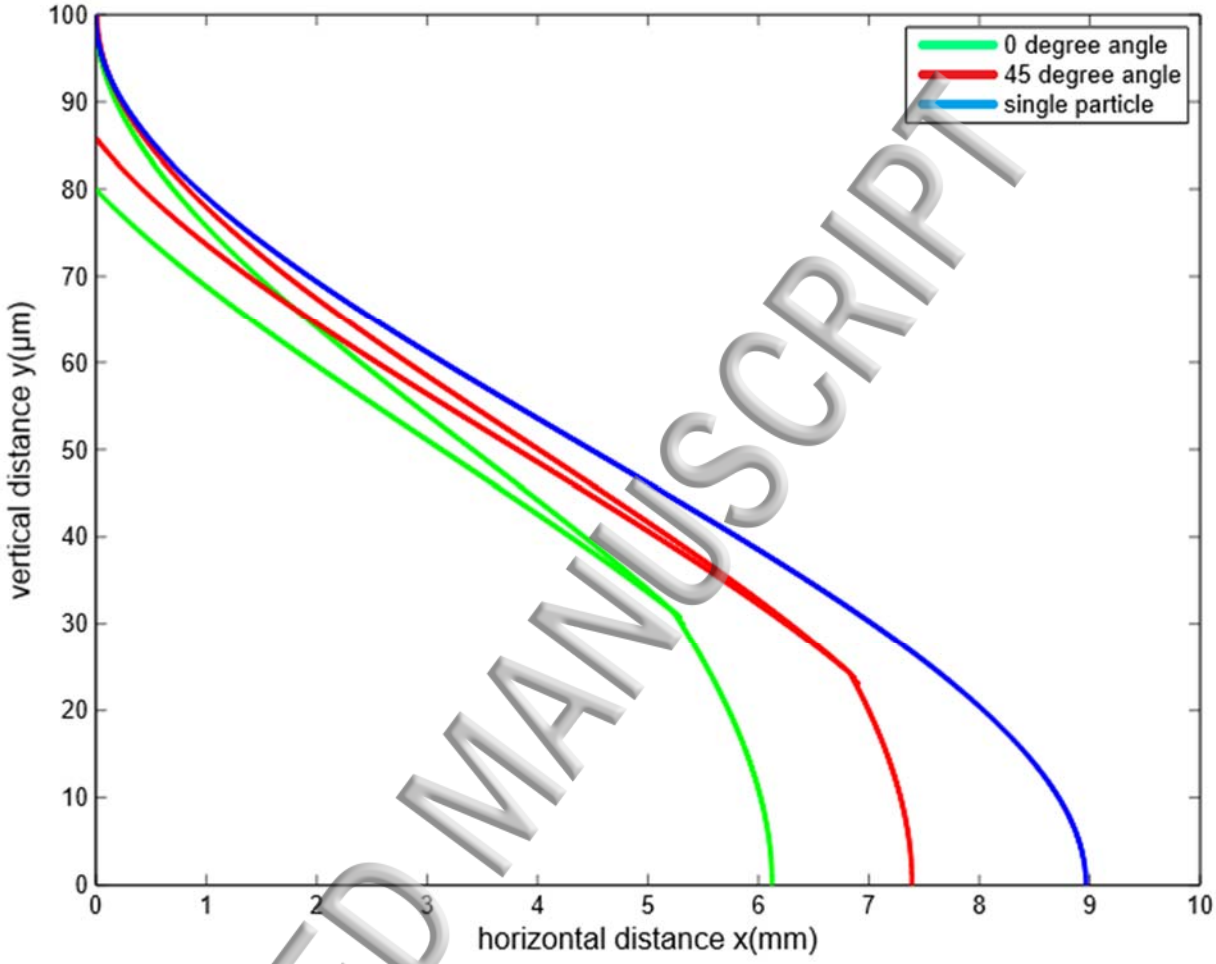

Figure 14 Comparison of trajectories of two cell-bead particle complexes with a single particle trajectory for cases where connector vector is parallel (0°) and at 45°angle with the applied magnetic field. The distance between particle complexes is twice that of the particle diameter (r=2D).

V. CONCLUSIONS

In this paper, a Lagrangian transport analysis was performed to predict trajectories of cell-bead particle complexes in a magnetophoretic bio-separation chip. A dipole-based model was employed to calculate the particle-particle interaction and obtain particle trajectories within the microfluidic device. Simulations were performed for three different cases where the geometric positions of the

particle complexes were parallel, at a 45 degrees angle, and perpendicular with the applied magnetic field. The parallel and perpendicular cases were selected because they represent two extreme cases where particles either fully attract or repel one another. While one could model any angles between 0 and 90, a 45 degrees angle was chosen because the interaction force is still attractive albeit much weaker than the zero degrees case. A parametric study was also performed to analyze the effect of particle-particle interaction on the trajectories of cell-bead complexes by varying flow rate, cell size, and number of beads per cell. The trapping length was observed to increase with increasing the flow rate and cell size while it decreased with increasing the number of beads per cell. It was found that the interaction force between cell-bead complexes can be attractive or repulsive depending on the angle between the magnetic moment and the connector vector. When the applied magnetic field is parallel to the connector vector, an attractive force between particle complexes are observed, causing the particles to join together and trap sooner than a single particle. However, if the magnetic moment and connector vector are perpendicular, the interaction force is repulsive, and the particles are repelled from each other and follow their own trajectories. In this case, particle-particle interaction force has a very little or no effect on the trapping length. It is also noticed that if the connector vector forms a 45° angle with the magnetic moment, a less dominant attractive force is produced between the particle complexes than the case where the magnetic moment is parallel with the connector vector. These modeling results provide valuable insights into a better understanding of particle-particle interaction and its effect on particle trajectory which cannot be easily obtained from experimental observations.

REFERENCES

1. V.I. Furdui and D.J. Harrison, “Immunomagnetic T cell capture from blood for PCR analysis using microfluidic systems,” Lab on a Chip 4, 614-618 (2004).

2. D.W. Inglis, R. Riehn, R.H. Austin, and J.C. Sturm, “Continuous microfluidic immunomagnetic cell separation,” Applied Physics Letters 85, 5093-5095 (2004).

3. M. Arruebo, R. Fernndez-Pacheco, M.R. Ibarra, and J. Santamara, “Magnetic nanoparticles for drug delivery,” Nano today 2, 22-32 (2007).

4. N. Xia, T.P. Hunt, B.T. Mayers, E. Alsberg, G.M. Whitesides, R.M. Westervelt, and D.E. Ingber, “Combined microfluidic-micromagnetic separation of living cells in continuous flow,” Biomedical Microdevices 8, 299-308 (2006).

5. N. Pamme and C. Wilhelm, "Continuous sorting of magnetic cells via on-chip free-flow magnetophoresis," Lab on a Chip 6 974-980 (2006).

6. E.P. Furlani, "Magnetophoretic separation of blood cells at the microscale," Journal of Physics D: Applied Physics 40, 1313 (2007).

7. J.D. Adams, U. Kim, and H.T. Soh, "Multitarget magnetic activated cell sorter," Proceedings of the National Academy of Sciences 105, 18165-18170 (2008).

8. K. Hoshino, Y.Y. Huang, N. Lane, M. Huebschman, J.W. Uhr, E.P. Frenkel, and X. Zhang, "Microchip-based immunomagnetic detection of circulating tumor cells," Lab on a Chip 11, 3449-3457 (2011).

9. T.P. Forbes and S.P. Forry, "Microfluidic magnetophoretic separations of immunomagnetically labeled rare mammalian cells," Lab on a chip 12, 1471-1479 (2012).

10. J. Zeng, Y. Deng, P. Vedantam, T.R. Tzeng, and X. Xuan, "Magnetic separation of particles and cells in ferrofluid flow through a straight microchannel using two offset magnets," Journal of Magnetism and Magnetic Materials 346, 118-123 (2013).

11. M. Hejazian, W. Li, and N.T. Nguyen, "Lab on a chip for continuous-flow magnetic cell separation," Lab on a Chip 15, 959-970 (2015).

12. O. Philippova, A. Barabanova, V. Molchanov, A. Khokhlov, "Magnetic polymer beads: Recent trends and developments in synthetic design and applications," Europ. Poly. Journal, **47**, 542-559 (2011).

13. J. Ugelstad, P. Stenstad, L. Kilaas, W. S. Prestvik, R. Herje, A. Berge, and E. Hornes, "Monodisperse magnetic polymer particles-new biochemical and biomedical applications," Blood Purif, **11**, 349 (1993).

14. Q. A. Pankhurst, J. Connolly, S. K. Jones and J. Dobson, "Applications of magnetic nanoparticles in biomedicine," J. Phys. D: Appl. Phys. 36, R167-R181 (2003).

15. K. Nandy, S. Chaudhuri, R. Ganguly, I. K. Puri, "Analytical model for the magnetophoretic capture of magnetic microspheres in microfluidic devices," Journal of Magnetism and Magnetic Materials, **320**, 1398-1405 (2008).

16. J. Darabi and C. Guo, "On-chip magnetophoretic isolation of CD4+ T cells from blood," Biomicrofluidics, **7**, 054106 (2013).

17. C. Hale and J. Darabi, "Magnetophoretic-based microfluidics device for DNA isolation," Biomicrofluidics, **8**, 044118 (2014).

18. S. S. Shevkoplyas, A. C. Siegel, R. M. Westervelt, M. G. Prentissc and G.M. Whitesides, "The force acting on a superparamagnetic bead due to an applied magnetic field," The Royal Society of Chemistry, Lab Chip, **7**, 1294-1302 (2007).

19. J. Zhu, L. Liang, X. Xuan, "On-chip manipulation of nonmagnetic particles in paramagnetic solutions using embedded permanent magnets," Microfluidics and Nanofluidics, **12**, 65-73 (2007).

20. I. Safarýk, M. Safarýkova, Scientific and Clinical Applications of Magnetic Carriers, ed. by U. Hafeli, W. Schutt, J. Teller, M. Zborowski, Plenum, New York, 323 (1997).

21. C. Mikkelsen, M. F. Hansen, and H. Bruus, "Theoretical comparison of magnetic and hydrodynamic interactions between magnetically tagged particles in microfluidic systems," Journal of Magnetism and Magnetic Materials, 293, 578-583 (2005).

22. R. Folkersmaa, H.N. Steina, F.N. Vosse, "Hydrodynamic interactions between two identical spheres held fixed side by side against a uniform stream directed perpendicular to the line connecting the spheres' centres," Int. J. of Multi. Flow, **26**, 877-887 (2000).

23. E. E. Keaveny, M. R. Maxey, "Modelling the magnetic interactions between paramagnetic beads in magnetorheological fluids," Journal of Computational Physics, **227**, 9554-9571 (2008).

24. D. Du, D. Li, M. Thakur, S. Biswal, "Generating an in situ tunable interaction potential for probing 2-D colloidal phase behavior," Soft Matter, **9**, 6867-6875 (2013).

25. N. Osterman, I. Poberaj, J. Dobnikar, D. Frenkel, P. Ziherl, D. Babić, "Field-Induced Self-Assembly of Suspended Colloidal Membranes," Phys. Rev. Lett.,**103**, 22-27 (2009).

26. U. Jeong, X. W. Teng, Y. Wang, H. Yang, Y. N. Xia, "Superparamagnetic colloids: controlled synthesis and niche applications," Adv. Materials, **19**, 33-60 (2007)

27. P. Tierno, O. Guell, F. Sagues, R. Golestanian, and I. Pagonabar-raga, "Controlled propulsion in viscous fluids of magnetically actuated colloidal doublets," Phys. Rev. E, 81, 011402 (2010)

28. Y. Gao, A. van Reenen, M.A. Hulsen, A.M. de Jong, M.W.J. Prins and J.M.J. den Toonder,"Disaggregation of microparticle clusters by induced magnetic dipole–dipole repulsion near a surface", Lab Chip, **13**, 1394-1401 (2013).

29. K. W. Yung, P. B. Landecker, D. D. Villani, "An analytic solution for the force between two magnetic dipoles", Magnetic and Electrical Separation, **9**, 39-52.

30. I.S. Grant and W.R. Phillips, Electromagnetism (2nd ed.), Manchester Physics, John Wiley & Sons. ISBN 978-0-471-92712-9, (2008).

31. D.J. Griffiths, Introduction to Electrodynamics (3rd ed.) Pearson Education, ISBN 81-7758-293-3, (2007).

32. J. Greene, F.G. Karioris, "Force on a magnetic dipole," American J. Physics, **39**, 172-175 (1970).

33. T.H. Boyer, "The force on a magnetic dipole," American J. Physics, **56**, 688-692 (1988).

34. K. R. Brownstein, "Force exerted on a magnetic dipole," American J. Physics, **61**, 940-941 (1988).

35. L. Vaidman, "Torque and force on a magnetic dipole," American J. Physics, **58**, 978-983 (1990).

36. S.A. Khashan, A. Alazzam, and E.P. Furlani, "Computational Analysis of Enhanced Magnetic Bio-separation in Microfluidic Systems with Flow-Invasive Magnetic Elements," Sci. Rep., **4**, 5299 (2014).

37. M.M. Clark, Transport Modeling for Environmental Engineers and Scientists (2nd ed.), John Wiley & Sons, New Jersey, ISBN-13: 978-0470260722 (2009)

38. M. Golozar, M. Molki, and J. Darabi, "Computational and performance analysis of a continuous magnetophoretic bioseparation chip with alternating magnetic fields," J. Microfluid Nanofluid 21: 73. https://doi.org/10.1007/s10404-017-1909-4 (2017).